Application of a Planetary Wave Breaking Parameterization to Stratospheric Circulation Statistics

WILLIAM J. RANDEL AND ROLANDO R. GARCIA

National Center for Atmospheric Research, Boulder, Colorado*

(Manuscript received 18 January 1993, in final form 9 September 1993)

ABSTRACT

The planetary wave parameterization scheme developed recently by Garcia is applied to stratospheric circulation statistics derived from 12 years of National Meteorological Center operational stratospheric analyses. From the data a planetary wave breaking criterion [based on the ratio of the eddy to zonal mean meridional potential vorticity (PV) gradients], a wave damping rate, and a meridional diffusion coefficient are calculated. The equatorward flank of the polar night jet during winter is identified as a wave breaking region from the observed PV gradients; the region moves poleward with season, covering all high latitudes in spring. Derived damping rates maximize in the subtropical upper stratosphere (the "surf zone"), with damping time scales of 3–4 days. Maximum diffusion coefficients follow the spatial patterns of the wave breaking criterion, with magnitudes comparable to prior published estimates. Overall, the observed results agree well with the parameterized calculations of Garcia.

1. Introduction

It is generally accepted that dissipation of planetary waves in the middle atmosphere is greatly enhanced by "breaking," that is, by the cascade of wave properties to small scales where they can be acted upon more readily by processes such as radiative damping and mixing. Wave breaking can be simulated in numerical models of sufficiently high spatial resolution, but it must be parameterized in lower-resolution models and indeed in two-dimensional models, where zonally asymmetric motions cannot be represented explicitly at all. In a recent paper, Garcia (1991, hereafter G91) has attempted to characterize the wave breaking process in terms of a dissipation rate, δ, derived from the linearized, steady-state equation for the conservation of planetary wave activity:

$$\delta = \frac{-\nabla\cdot(\mathbf{C}_g A)}{2A}, \qquad (1)$$

where $\mathbf{C}_g$ represents the group velocity and A is the quasigeostrophic wave activity density (also known as the angular pseudomomentum). The idea embodied in Eq. (1) is that, in regions where the wave amplitude exceeds some "saturation" criterion, excess wave activity must be dissipated at a rate dictated by the convergence of wave activity flux, $\nabla\cdot(\mathbf{C}_g A)$, into the region. Garcia also showed that, under certain assumptions, one can derive a horizontal diffusion coefficient, K_{yy}, as a function of δ. This approach has the advantage of providing mutually consistent estimates of the effect of planetary wave breaking on the mean meridional circulation and on diffusive transport.

In addition to its possible application to low-resolution models of the middle atmosphere, Garcia's treatment of wave breaking is of interest in that it provides a simple conceptual framework for interpreting why wave breaking occurs and how its distribution changes as a function of location, season, and the strength of wave forcing. Following results of other authors (e.g., Haynes 1989), the parameterization is based on the assumption that barotropic instability is the mechanism that precipitates wave breaking. Wave saturation, and hence wave breaking, is assumed to occur in those regions where the eddy potential vorticity gradient exceeds the background zonal mean value, that is, in regions where the necessary condition for barotropic instability (Charney and Stern 1962) is met. The parameterization also identifies wave group velocity as the most important factor determining the dissipation rate due to breaking, as per Eq. (1).

As noted by G91, this simple approach to parameterizing wave breaking yields physically plausible results for the dissipation rate, δ, and for the horizontal diffusion coefficient derived from the dissipation rate. In particular, the magnitude of δ agrees well with estimates obtained from high-resolution numerical models (e.g., Robinson 1988) and from the observational

* The National Center for Atmospheric Research is sponsored by the National Science Foundation.

Corresponding author address: Dr. William J. Randel, NCAR, P.O. Box 3000, Boulder, CO 80307-3000.

study of Randel (1990). The derived diffusion coefficients are also consistent with recent work (e.g., Plumb and Mahlman 1987; Juckes 1989; Salby et al. 1990; Yang et al. 1990). In spite of this good overall agreement, the parameterization has not been tested extensively on stratospheric observations. The purpose of this paper is to make such detailed comparisons with climatological data for the stratosphere. We utilize National Meteorological Center (NMC) daily stratospheric analyses on pressure levels between 100 and 1 mb for the years 1979–1990. These data cover a period long enough to establish a stratospheric climatology against which the results of the wave breaking parameterization can be compared. Agreement between the numerical results of G91 and those obtained from the NMC data would enhance our confidence in the former and provide a simple theoretical basis for the interpretation of the latter.

Section 2 of the paper describes the NMC dataset and the methods used to analyze it. Estimates of dissipation rates and diffusion coefficients due to wave breaking, their spatial distribution, and seasonal evolution are presented in section 3. The results are contrasted with the predictions of Garcia's parameterization and with estimates of stratospheric diffusion coefficients obtained by other authors. A summary and discussion are provided in the last section.

2. Data and analyses

The data to be examined are daily stratospheric geopotential height analyses produced at NMC, available on pressure levels of 100, 70, 50, 30, 10, 5, 2, and 1 mb. These height fields are used to derive hydrostatic temperatures and linear balance horizontal winds, as described in Randel (1992). Because the focus here is on the quasigeostrophic equations, and because eddy wind derivations are problematic in the tropics, we show results only poleward of 20° in each hemisphere. Climatological averages shown here are taken over the 12 years, 1979–1990.

This paper examines several highly derived quantities related to the quasigeostrophic potential vorticity (PV) fields. The zonal mean PV gradient $\overline{q}_y$ is given by:

$$\overline{q}_y = \frac{2\Omega}{a}\cos\phi - \frac{1}{a^2}\frac{\partial}{\partial\phi}\left[\frac{1}{\cos\phi}\frac{\partial}{\partial\phi}(\overline{u}\cos\phi)\right] - (2\Omega\sin\phi)^2 e^{z/H}\frac{\partial}{\partial z}\left[e^{-z/H}\frac{1}{N^2}\frac{\partial\overline{u}}{\partial z}\right], \quad (2)$$

where notation is standard, following Andrews et al. (1987). The vertical coordinate is $z = H\ln(1000\text{ mb}/p)$, with H a constant scale height of 7 km. Throughout this paper, overbars denote zonal means and primes deviations therefrom. The eddy potential vorticity, q', follows the definition of Palmer (1982):

$$q' = \frac{1}{a}\left[\frac{1}{\cos\phi}\frac{\partial v'}{\partial\lambda} - \frac{\sin\phi}{\cos\phi}\frac{\partial}{\partial\phi}\left(\frac{\cos\phi}{\sin\phi}u'\right)\right] + 2\Omega\sin\phi e^{z/H}\frac{\partial}{\partial z}\left[e^{-z/H}\frac{R}{HN^2}T'\right]. \quad (3)$$

Because the NMC data are archived as zonal Fourier components on a latitude–pressure grid, zonal derivatives are calculated spectrally, while latitude and pressure derivatives are calculated using finite-difference approximations. Also, due to the large number of derivatives involved in (2)–(3), a 1–2–1 meridional smoothing was applied to the resultant fields.

One fundamental difficulty arises in the comparisons because the parameterization scheme of G91 is derived for a single zonal wave component, whereas observed stratospheric variability has significant contributions from at least zonal waves 1 and 2. A straightforward way around this difficulty is to assume that the individual zonal waves do not attain large amplitudes simultaneously and sum the contributions from the individual waves for a total wave effect. Although such an idealized situation is not always realized, it is nevertheless fairly consistent with observations (e.g., Smith et al. 1984), and we proceed assuming such a separation.

The criterion for planetary Rossby wave breaking defined by Garcia is that the eddy PV gradient exceeds the zonal mean PV gradient, that is,

$$|q'_y|/\overline{q}_y > 1. \quad (4)$$

The rationale is that when this criterion is satisfied, the total PV gradient ($\overline{q}_y + q'_y$) will be negative, which is a necessary condition for barotropic instability (Charney and Stern 1962). Numerical simulations (e.g., Haynes 1989) indicate that barotropic instability plays an important role in the development of Rossby wave critical layers, and thus in Rossby wave breaking. Here we calculate $|q'_y|$ as a sum over a band of zonal wave numbers, k, according to:

$$|q'_y| = \frac{1}{a}\left\{\sum_{k=1}^{4}\left[\left(\frac{\partial s_k}{\partial\phi}\right)^2 + \left(\frac{\partial c_k}{\partial\phi}\right)^2\right]\right\}^{1/2}, \quad (5)$$

where s_k and c_k are the zonal sine and cosine coefficients of the eddy PV defined in (3). Because we are interested mainly in locating regions where the eddy gradients are large (as opposed to locations where the zonal mean gradients are very small or negative, which signals instability of the zonal mean flow) we have, more or less arbitrarily, set a minimum value of $\overline{q}_y$ at 0.5×10^{-11} m^{-1} s^{-1} when calculating the ratio (4).

Some results for a particular day with a large amplitude wave in the stratosphere (14 January 1990) are presented here as an example. Figures 1a–c show the zonally averaged zonal wind, $\overline{u}$, the zonally averaged PV gradient, $\overline{q}_y$, and amplitude of the eddy PV gradient, $|q'_y|$. Relatively large values of $\overline{q}_y$ are found along

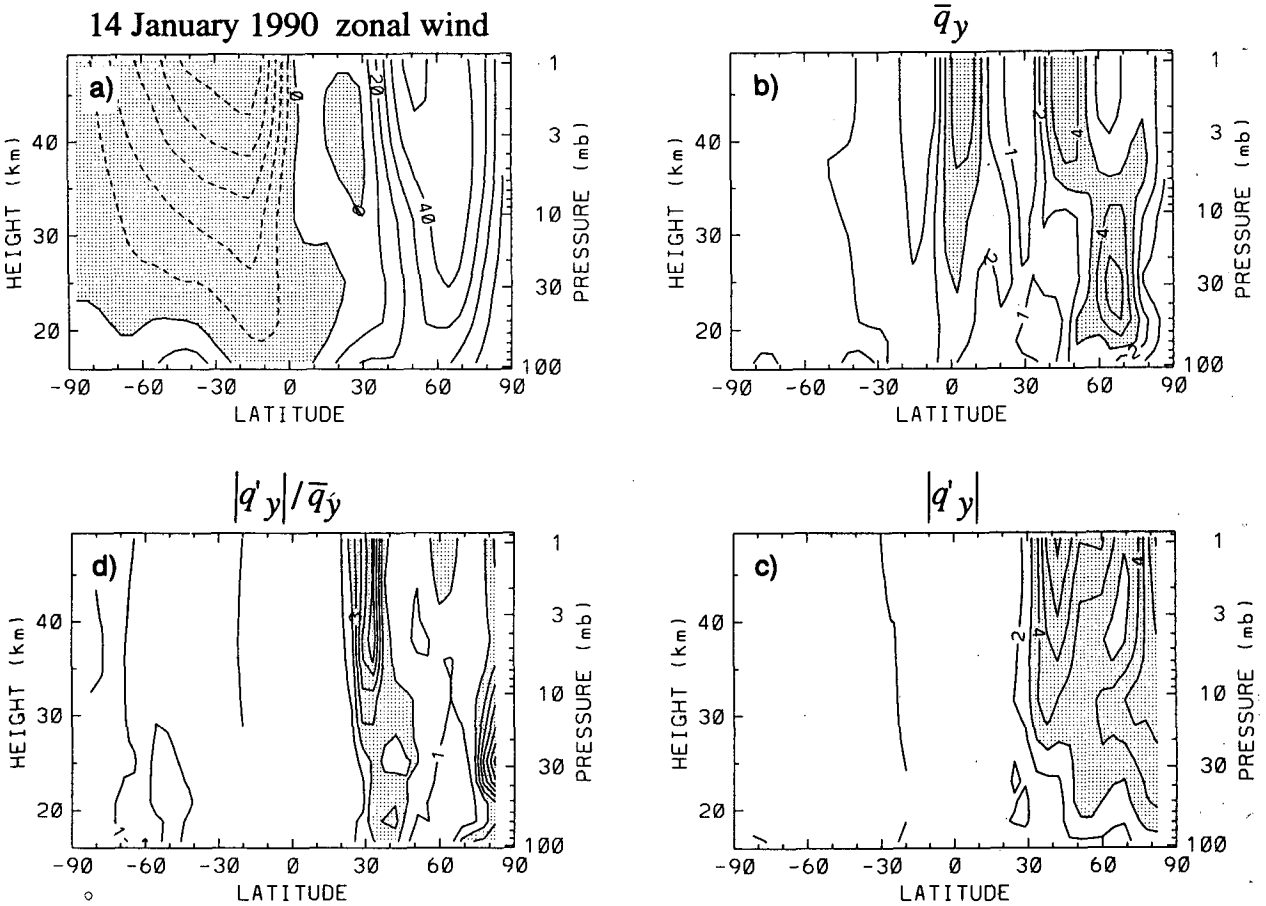

FIG. 1. Meridional cross sections of zonal average quantities on 14 January 1990. (a) Zonal wind $\bar{u}$, (b) zonal mean PV gradient $\bar{q}_y$, (c) amplitude of eddy PV gradient $|q'_y|$, (d) ratio of $|q'_y|/\bar{q}_y$. Units in (b)–(c) are 10^{-11} m^{-1} s^{-1}, with values above 3.0 shaded.

the axis of the polar night jet, with small values on the north and south flanks. Figure 1d shows the ratio of the eddy to zonal mean PV gradients for this day, based on the individual cross sections shown in Figs. 1b–c. The ratio exhibits a strong maximum in the subtropics between 20° and 40°N, with values in excess of 4 above 10 mb at 35°N. Figure 2a presents a synoptic map of the 10-mb geopotential height for this day, showing an enhanced Aleutian anticyclone, and the center of the vortex displaced slightly off the pole. The local meridional PV gradient, $(\overline{q_y} + q'_y)$, is shown in Fig. 2b. A large region of negative gradient wraps around the equatorward side of the anticyclone; this is the local manifestation of the region where the criterion (4) is met in Fig. 1d. Note that there is also a region of negative meridional PV gradient near the pole in Fig. 2b, and a corresponding region of ratio $|q'|/\overline{q_y} > 2$ over polar latitudes in Fig. 1d. This is a result of the vortex center being moved off the pole, a situation quite distinct from the reversals at low latitudes, which are due to planetary wave advective effects. These reversed PV gradients in polar regions occur often (see Baldwin and Holton 1988, their Fig. 3), and because we do not wish to include them as wave breaking regions, we simply do not plot the ratio (4) polewards of 64° latitude in our climatological results.

A more rigorous identification of wave breaking regions may be made by examining the meridional gradient of Rossby–Ertel PV,

$$Q = -g(\zeta + f)\frac{\partial \theta}{\partial p}, \qquad (6)$$

calculated on isentropic surfaces (McIntyre and Palmer 1983, 1984; Clough et al. 1985). For comparison to the quasigeostrophic results, we show in Fig. 3a the Rossby–Ertel PV Q for this day on the 850-K isentrope (near the 10-mb level); Fig. 3b shows the meridional gradient of Q. Comparison to the 10-mb quasigeostrophic calculations (Fig. 2b) shows that the regions of reversed gradient are nearly identical. This similarity enhances our confidence in the use of quasigeostrophic theory in the Rossby wave parameterization.

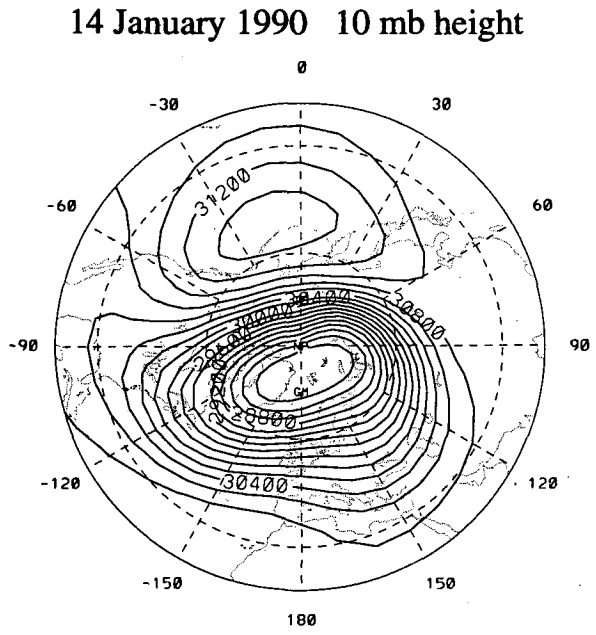

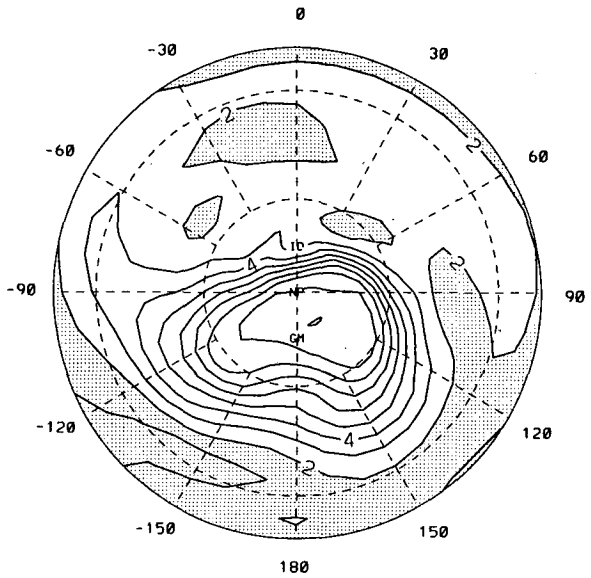

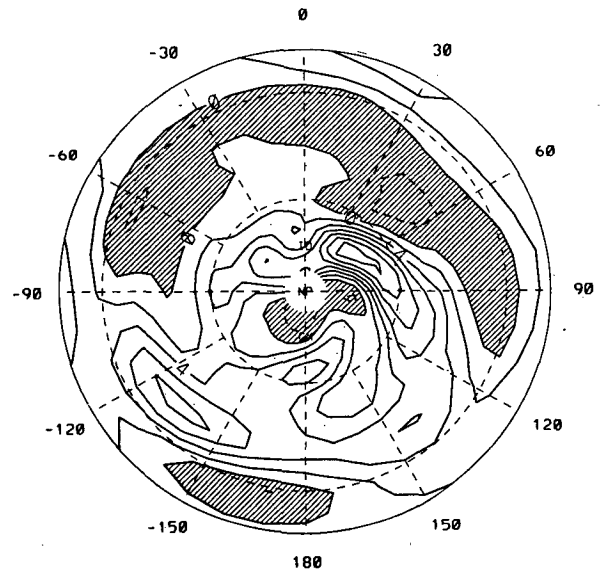

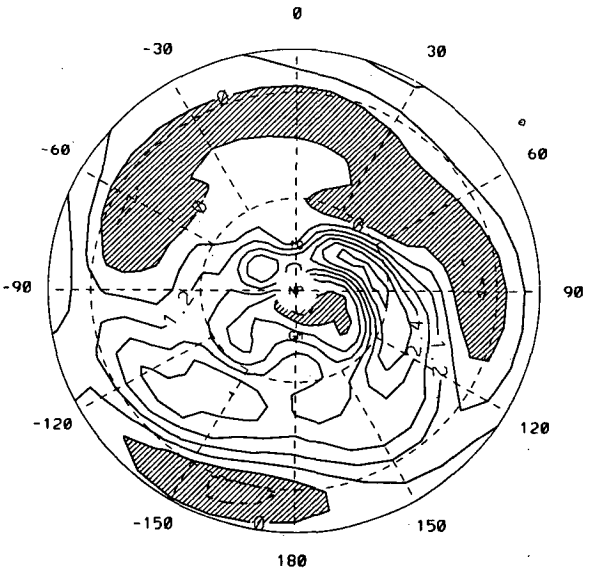

FIG. 2. Polar stereographic maps of 10-mb geopotential height (m) and quasigeostrophic PV gradient (10^{-11} m^{-1} s^{-1}) for 14 January 1990. Regions of negative PV gradient are hatched.

FIG. 3. Polar stereographic maps of the Rossby–Ertel potential vorticity on the 850-K potential temperature surface (PV units of 10^{-5} K m^2 kg^{-1} s^{-1}), and its calculated meridional gradient (PV units/500 km), for 14 January 1990. Regions of negative PV gradient are hatched. Note the close correspondence to the 10-mb quasigeostrophic PV gradient shown in Fig. 2.

The planetary wave damping rate δ is calculated from Eq. (1), with the quasigeostrophic wave activity density A given by (Palmer 1982):

$$A = \frac{1}{2} a \cos\phi e^{-z/H} \overline{q'^2} / \overline{q_y}. \qquad (7)$$

We furthermore use the fact that, for linear Rossby waves that obey WKB scaling, the divergence of wave activity flux in (1) is proportional to the quasigeostrophic Eliassen–Palm (EP) flux divergence (Palmer 1982):

$$\nabla\cdot(\mathbf{C}_g A) = \nabla\cdot\mathbf{F}, \tag{8}$$

with

$$F_\phi = a\cos\phi e^{-z/H}\left[-\overline{u'v'} - \frac{R}{H}\frac{\partial\bar{u}}{\partial z}\frac{\overline{v'T'}}{N^2}\right]$$

$$F_z = a\cos\phi e^{-z/H}\left[\hat{f}\frac{R}{H}\frac{\overline{v'T'}}{N^2}\right], \tag{9}$$

and

$$\hat{f} = f - \frac{1}{a\cos\phi}\frac{\partial}{\partial\phi}(\bar{u}\cos\phi).$$

Combining (1), (7), and (8), our estimate of the damping rate is given by

$$\delta = -\frac{\mathrm{DF}}{(\overline{q'^2}/\overline{q_y})}, \tag{10}$$

where DF is the scaled EP flux divergence

$$\mathrm{DF} = \frac{e^{z/H}}{a\cos\phi}\nabla\cdot\mathbf{F} \tag{10a}$$

in units of meters per second per day.

We require the damping rate for individual zonal wavenumbers in the expression for the diffusion coefficient given below. We find that the derived values for each wavenumber are approximately the same, and for ease of calculation (10) is estimated using the numerator and denominator each summed over the zonal wave band; this gives values similar to the results for individual wavenumbers. We calculate the ratio in (10) using time-averaged quantities (as described below), because this equation is derived from the steady-state wave activity equation (1), that is, the effects of daily wave transience are not considered. In order for the wave activity A (7) to be well behaved, we also require $\bar{q}_y \geq 0.5\times10^{-11}$ m^{-1} s^{-1} in calculating (10).

According to G91, the derived damping coefficient δ(10) can be used to estimate an eddy diffusion coefficient:

$$K_{yy} = \frac{\delta\overline{v'v'}}{k^2(\bar{u}-c)^2+\delta^2}, \tag{11}$$

where k and c are the (dimensional) zonal wavenumber and phase speed of the planetary wave. Using the steady-state meridional eddy displacement, $\eta' = -iv'/(k(\bar{u}-c))$, this expression may also be written as

$$K_{yy} = \delta\overline{\eta'\eta'}\Big/\left[1+\left(\frac{\delta}{k(\bar{u}-c)}\right)^2\right]. \tag{12}$$

We calculate (12) for each zonal wave coefficient (by calculating $\overline{\eta'\eta'}$ for each wavenumber), and the total K_{yy} shown here is given by the sum over the individual wavenumbers. In order to keep (12) well behaved near critical lines (where $\bar{u} = c$), we enforce two restrictions: 1) $|\eta'| \leq 1500$ km, and 2) $|\bar{u}-c| \geq 3$ m s^{-1}. Our results are not sensitive to the exact values of these limits.

The parameterized eddy diffusion coefficient, K_{yy}, given by (12) can be compared to estimates, D_{yy}, derived from the closure assumption

$$\overline{v'q'} = -D_{yy}\bar{q}_y, \tag{13}$$

which expresses a simple flux gradient relationship for quasigeostrophic PV. Using the fact (Palmer 1982) that, for quasigeostrophic waves, $\overline{v'q'} = \mathrm{DF}$, where DF is the scaled EP flux divergence (10a), Eq. (13) becomes

$$D_{yy} = -\mathrm{DF}/\bar{q}_y. \tag{14}$$

Newman et al. (1988) have estimated D_{yy} from the NMC data according to (14), using a linear regression (with zero intercept) of monthly mean $\overline{v'q'}$ and $\bar{q}_y$ values. Here we simply calculate the ratio (14) from long-term average fields, again using the requirement that $\bar{q}_y \geq 0.5\times10^{-11}$ m^{-1} s^{-1}. The direct ratio method of calculating (14) gives maximum values in the subtropics (see below), versus maxima in high latitudes calculated by Newman et al. (1988). Observational and theoretical studies (Plumb and Mahlman 1987; Juckes 1989; Salby et al. 1990; Yang et al. 1990; Sassi et al. 1990; G91; Stanford et al. 1993) indicate that maximum Rossby wave mixing and associated diffusion occur in the subtropics.

The parameterized diffusion coefficient (12) and the flux gradient expression (14) may be shown to be equivalent if the observed waves obey the linearized potential vorticity equation

$$ik(\bar{u}-c)q'_{\mathrm{lin}} + v'\bar{q}_y = -\delta q'_{\mathrm{lin}}, \tag{15}$$

whence

$$\overline{q'^2_{\mathrm{lin}}} = -\overline{\eta'\eta'}\,\bar{q}_y^{\,2}\Big/\left[1+\left(\frac{\delta}{k(\bar{u}-c)}\right)^2\right], \tag{16}$$

where the substitution $v' = ik\eta'(\bar{u}-c)$ has been made.

Equations (10), (12), and (16) may be combined to rewrite the parameterized diffusion coefficient as

$$K_{yy} = -\frac{\mathrm{DF}}{\bar{q}_y}(\overline{q'^2_{\mathrm{lin}}}/\overline{q'^2_{\mathrm{obs}}}) \tag{17}$$

or, by (14),

$$K_{yy} = D_{yy}(\overline{q'^2_{\mathrm{lin}}}/\overline{q'^2_{\mathrm{obs}}}), \tag{18}$$

where $\overline{q'^2_{\mathrm{obs}}}$ are the values calculated from observations via (3). To the degree that $\overline{q'^2_{\mathrm{lin}}} = \overline{q'^2_{\mathrm{obs}}}$, the parameterized, K_{yy}, and flux gradient, D_{yy}, expressions for the diffusion coefficient are equivalent.

Time-average quantities are used to calculate the individual terms in (10), (12), and (14). The $|q'_y|/\bar{q}_y$ ratios in (4) are calculated daily and then averaged with respect to time. We note that nearly identical patterns

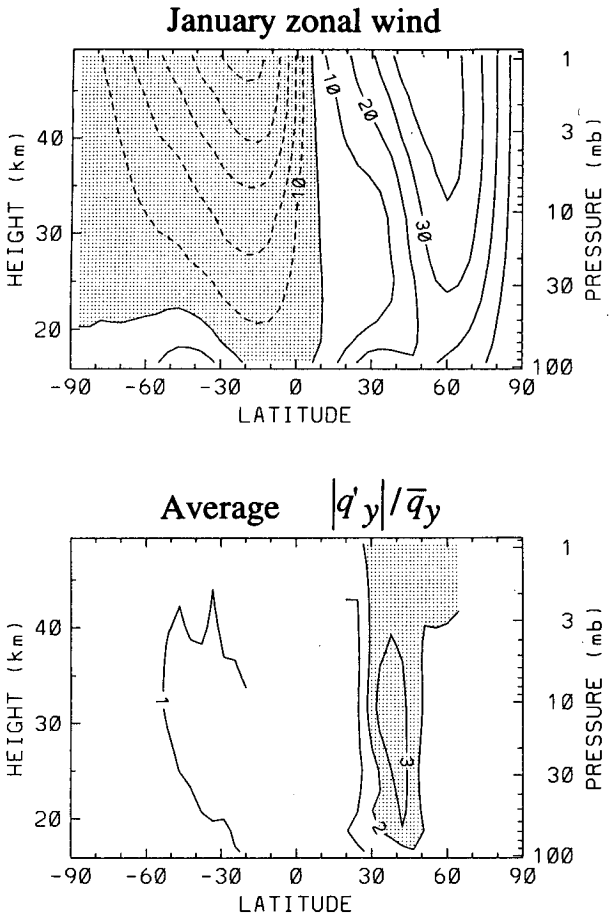

FIG. 4. January average zonal mean zonal wind $\bar{u}$ and average of the daily ratio $|q_y'|/\bar{q}_y$. Averages are calculated over the 12 years 1979–1990.

are found for (4) if the fields $|q_y'|$ and $\bar{q}_y$ are time averaged before taking their ratio, but the magnitudes are slightly smaller in that case. Direct time-averaged monthly means for January and August are shown below, along with climatological latitude–time sections in which the individual terms have been smoothed using a running Gaussian-shaped filter with a width of approximately one month (to approximate moving monthly means).

3. Results

a. January and August monthly means

Figure 4 shows the climatological average January mean zonal wind $\bar{u}$ and average ratio $|q_y'|/\bar{q}_y$. Maximum $|q_y'|/\bar{q}_y$ ratios (above 3) are found on the equatorward side of the jet in the middle stratosphere, where $\bar{q}_y$ is relatively small (see Fig. 1b). Almost the entire NH extratropics exhibit $|q_y'|/\bar{q}_y$ ratios greater than 1. Isolines of $|q_y'|/\bar{q}_y = 2$, on the other hand, correspond more nearly to expectations of the location of the subtropical wave breaking region. Note that a ratio of 1 would identify regions of marginal instability, where $(\bar{q}_y + q_y') = 0$, whereas a ratio of 2 would indicate regions where $(\bar{q}_y + q_y') < -\bar{q}_y$, that is, where the waves would reverse the sign of the background PV gradient. Identifying wave breaking regions according to $|q_y'|/\bar{q}_y > 2$ is somewhat arbitrary but qualitatively similar to the choice of Baldwin and Holton (1988, see their Fig. 2), who identified wave breaking by a certain maximum value of PV, together with a reversed meridional PV gradient. In fact, the region of $|q_y'|/\bar{q}_y > 2$ seen in Fig. 4 is very similar to the climatological latitudinal wave breaking profile identified by Baldwin and Holton (1988, their Fig. 3). Hereafter we replace (4) by

$$|q_y'|/\bar{q}_y > 2 \tag{19}$$

as our wave breaking criterion.

Figure 5 shows the calculated damping rate δ for January climatology. Note that we have chosen to contour values of δ only over regions where the magnitude of the EP flux divergence DF (10a) is greater than 0.5 m s^{-1}/day. The derived damping rates exhibit largest values in the subtropical upper stratosphere, with maxima on the order of 0.25–0.3 day^{-1} (corresponding to planetary wave damping time scales of 3–4 days). These magnitudes compare well with the maximum values of 0.3–0.4 day^{-1} calculated by G91. The largest damping rates obtained here are located slightly equatorward of the subtropical maximum in DF (not shown), and of the largest ratios of $|q_y'|/\bar{q}_y$, both of which peak near 30°–40° latitude. Note that these damping rates are computed directly from the ratio (10), whereas in G91 δ was obtained in terms of the WKB approximation for the group velocity, C_g, and wave activity density, A. The agreement between the damping rates obtained here and those of Garcia con-

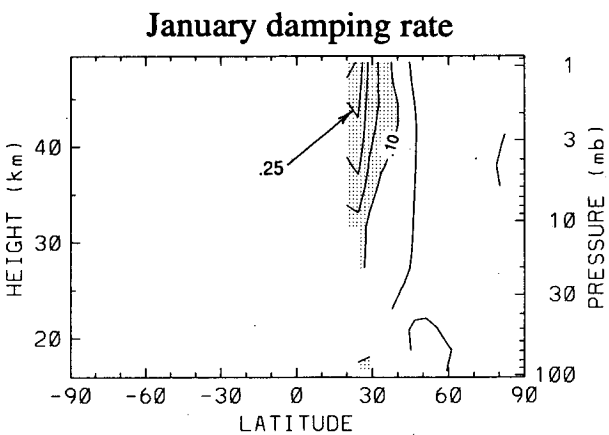

FIG. 5. Derived planetary wave damping rate δ (units of day^{-1}), calculated from January climatological data. Results are plotted only over regions where the climatological DF ≤ -0.5 m s^{-1}/day.

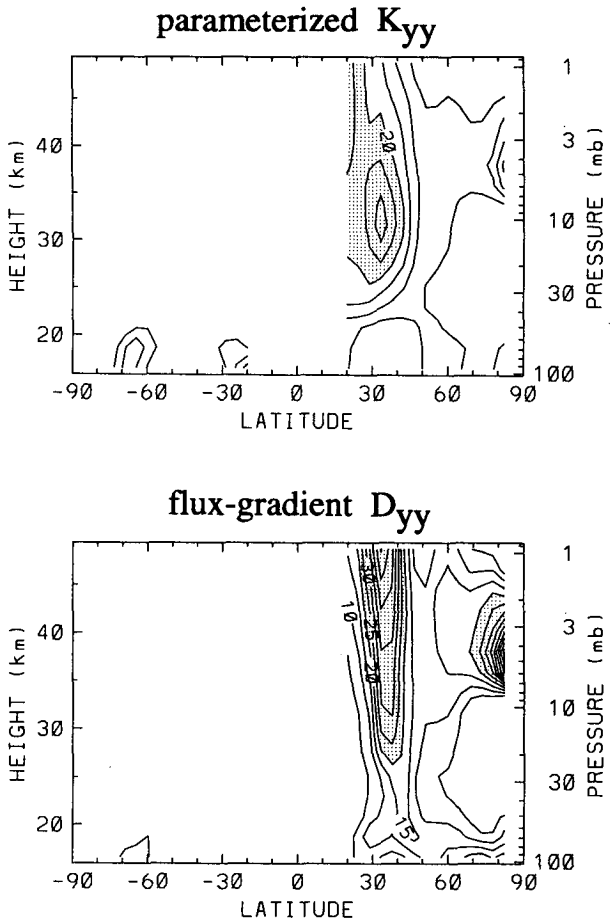

FIG. 6. Parameterized diffusion coefficient, K_{yy} (top), and flux gradient estimate, D_{yy} (bottom), calculated from January climatological data. Contours are 5×10^5 m^2 s^{-1}, with values above 20 shaded.

stitute a posteriori support for his use of the WKB approximation to express the dissipation rate.

Figure 6 shows the parameterized diffusion coefficient computed from Eq. (12), K_{yy}, along with the diffusion coefficient, D_{yy}, derived from the flux gradient relationship (14). Maxima in both estimates are found in the subtropics (20°–40°) and also in the polar upper stratosphere. Here K_{yy} reaches a maximum of about 30×10^5 m^2 s^{-1} in the middle stratosphere and decreases with height, while D_{yy} has a similar value at 10 mb, but increases with height to approximately 45×10^5 m^2 s^{-1} near 1 mb. The occurrence of subtropical maxima in the 20°–40° latitude range, with values of 30–40 ($\times 10^5$ m^2 s^{-1}), is consistent with prior estimates of diffusion coefficients from satellite observations [Lyjak (1987) and Sassi et al. (1990) using LIMS data; Yang et al. (1990) using NMC data; and Stanford et al. (1993) using SAMS data], and also with model calculations (Plumb and Mahlman 1987; Juckes 1989; Salby et al. 1990). Juckes (1989) and Stanford et al. (1993) also show a polar maximum in the diffusion coefficient similar to that in Fig. 6. The model calculations of G91, based on Eq. (12), show subtropical maxima in K_{yy} of approximately 20×10^5 m^2 s^{-1} (determined mainly by the structure of the derived wave breaking criterion). Garcia does not find a polar maximum in K_{yy} because his wave breaking criterion (4) is not satisfied in that region.

Derived statistics for SH winter (August) are shown in Figs. 7–9. The August zonal wind $\bar{u}$ (and also $\bar{q}_y$) has a much stronger high-latitude maximum compared to NH winter. The $|q_y'|/\bar{q}_y$ ratio shows a narrow maximum on the subtropical flank of the jet, centered near 30°–40° latitude. The derived wave breaking region in SH winter (Fig. 7b) is considerably narrower than that in NH winter (Fig. 4b), presumably because the larger amplitude waves observed in the NH are able to erode the polar vortex more effectively and so increase the width of the breaking region. A similar result is obtained by G91 (his Fig. 5).

The derived damping rate δ in the SH winter, shown in Fig. 8, maximizes in the subtropical upper stratosphere with values near 0.25, very similar in structure

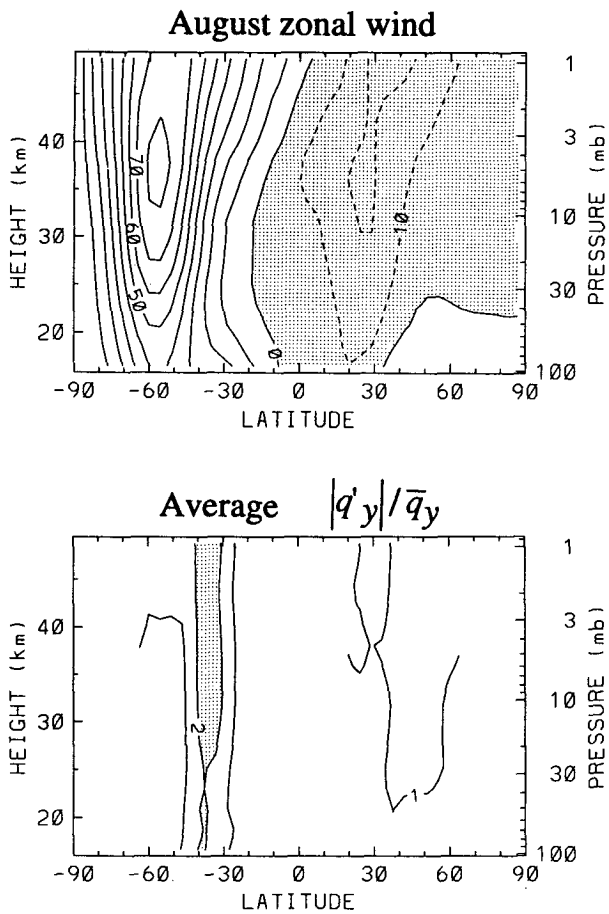

FIG. 7. August climatological zonal wind $\bar{u}$ and average ratio $|q_y'|/\bar{q}_y$.

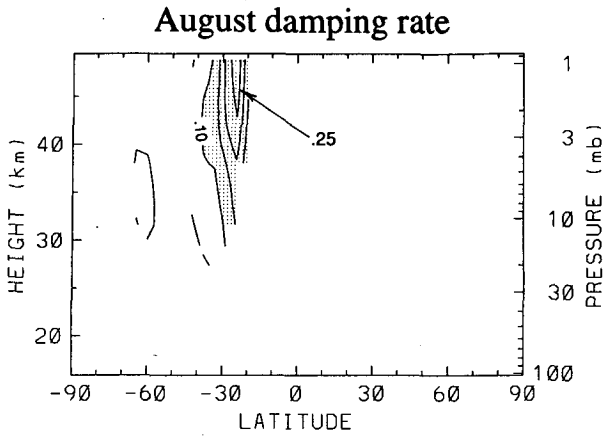

FIG. 8. August climatological planetary wave damping rate (units of day^{-1}). Results are only plotted over regions where the climatological DF ≤ -0.5 m s^{-1}/day.

and magnitude to the NH values (Fig. 5). As in the NH, the strongest damping rates are calculated somewhat equatorward of largest DF and $|q_y'|/\bar{q}_y$ ratios. Figure 9 shows the diffusion coefficients obtained from the parameterization (12) and the flux gradient relationship (14). The patterns are similar to those in the NH (Fig. 6), except that the parameterized diffusion, K_{yy}, shows maximum values at the lowest latitude included in the calculations (20°S). Estimates of K_{yy} for the NH (Fig. 6a), and of D_{yy} for both hemispheres (Figs. 6b, 9b), maximize at 30°–40°. This difference in latitudinal structure in Fig. 9 is due primarily to a combination of the background zonal wind profile (Fig. 7a) and the choice $c = 0$ for the zonal phase speed. Choosing $c = 10$ m s^{-1} [a realistic choice for the eastward propagating waves observed in the SH stratosphere—see the phase speed spectra of EP flux divergence shown in Fig. 8 of Randel and Held (1991)] results in the parameterized K_{yy} structure shown in Fig. 10, where the latitudinal maximum in the middle stratosphere has shifted to near 30°.

b. *Observed seasonal variations*

Seasonal evolution of the wave breaking criterion ($|q_y'|/\bar{q}_y > 2$) is shown in Fig. 11, superimposed on the zonal wind structure, for the 10-mb and 1-mb levels. The wave breaking patterns are basically the same at both levels: maxima are found in both hemispheres during middle to late winter on the equatorward flank of the polar night jet. The patterns move poleward and broaden during late winter–spring, so that all latitudes poleward of approximately 40° satisfy the criterion during these times. This seasonal evolution is intuitively consistent with subtropical wave breaking in midwinter, followed by broad latitudinal-scale disruption of the vortex during the spring transition. Note how the wave breaking region in the Southern Hemisphere is confined to middle latitudes until late winter, when it spreads beyond 60°S. Similar seasonal behavior is obtained by the model simulation of Garcia.

It could be argued that the agreement between the results of Fig. 11 and the calculations of G91 is to be expected insofar as Garcia's model produces a realistic seasonal cycle of zonal winds and wave amplitudes. However, such a realistic seasonal cycle is obtained in the model only when the planetary wave parameterization is employed. If the only dissipation mechanism included in the wave equation is thermal damping, it is found that the EP flux divergence is confined mainly to the upper stratosphere, where thermal relaxation is rapid. As a consequence, the model becomes very sensitive to wave forcing, producing frequent sudden warmings in both hemispheres even when climatologically realistic wave amplitudes are specified at the lower boundary. It appears, then, that the role of the parameterized damping rate in G91 is to allow significant wave dissipation to occur in the lower strato-

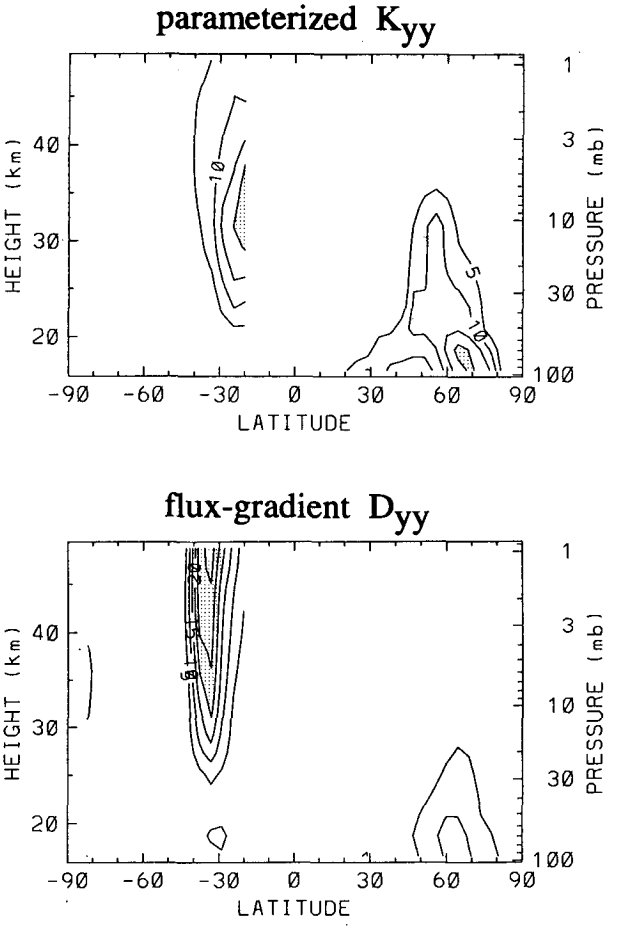

FIG. 9. Parameterized, K_{yy}, and flux gradient, D_{yy}, estimates of the diffusion coefficient derived from climatological data for August. Contours are 5×10^5 m^2 s^{-1}. The parameterized diffusivity, K_{yy}, is calculated using $c = 0$.

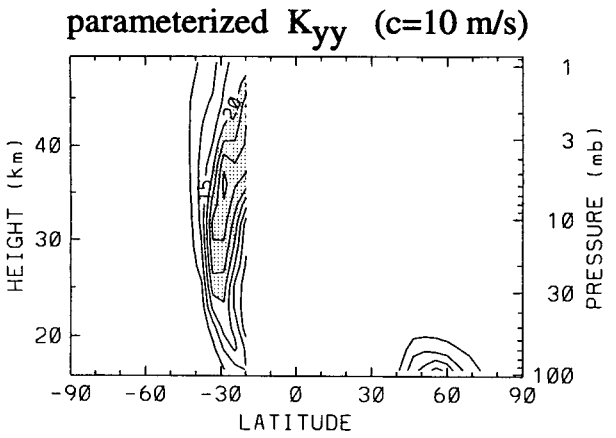

FIG. 10. Parameterized K_{yy} for August climatology, calculated using $c = 10$ m s^{-1}.

sphere, where its effects are less dramatic than in the upper stratosphere. The realistic seasonal evolution of the wave and mean state thus obtained, and the fact that the location and evolution of the breaking region agree with those determined from observations, may then be viewed as providing indirect support for the wave breaking parameterization.

The magnitude of the derived damping rates shows relatively little seasonal variation. Maximum values are observed in the subtropical upper stratosphere throughout both winter hemispheres, with magnitudes of 0.25–0.30 day^{-1}, similar to the patterns for January and August shown in Figs. 5 and 8, respectively. A weak maximum (~0.07 day^{-1}) is found at high latitudes during the spring transition in the SH (October–November), but not in the NH. This finding is also consistent with the conclusion of G91 that damping rates are essentially independent of wave amplitude, being determined instead by wave group velocity.

Figure 12 shows the seasonal variation of the parameterized and flux gradient estimates of the diffusion coefficient at 10 mb. Here we have used a zonal phase speed $c = 0$ in the NH and $c = 10$ m s^{-1} in the SH, close to values derived from observed transient wave statistics (Randel and Held 1991, Fig. 8). The two estimates shown in Fig. 12 are very similar. This follows from the fact that the two expressions for the diffusion coefficient, (12) and (14), are equivalent if $\overline{q'^2_{\text{lin}}} = \overline{q'^2_{\text{obs}}}$ (18), which apparently is the case at 10 mb. The evolution is similar in pattern to that of the wave breaking criterion (Fig. 11), with maxima over 30°–40° during midwinter, moving poleward during late winter–spring. High-latitude mixing (large values of the diffusion coefficient) is found in spring in both hemispheres.

Figure 13 shows seasonal variation of the two estimates of the diffusion coefficient at 2 mb. Overall, the seasonality is similar to that at 10 mb; however, the parameterized values, K_{yy}, are approximately only half as large in the subtropics as the flux gradient results, D_{yy}. The results in Fig. 13 imply that the linearized PV estimates q'_{lin} are too small compared to observed values in the upper stratosphere. This could happen if the damping rate obtained from (10) were an overestimate of the "true" damping rate due to wave breaking. Thermal damping rates are fast in the middle stratosphere, so thermal dissipation may contribute substantially to the EP flux divergence there. If this is the case, DF in Eq. (10) would overestimate the EP flux divergence due solely to wave breaking and this, in turn, would yield too small a value of q'_{lin}.

4. Summary and discussion

The purpose of this study has been to apply the simple equations derived by G91 to observational data to

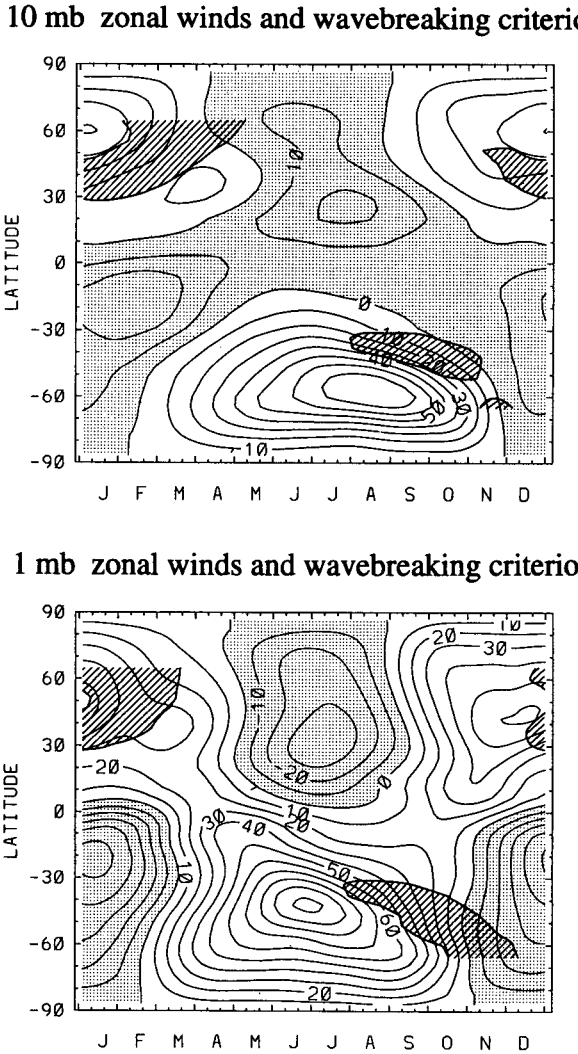

FIG. 11. Climatological latitude–time sections of derived wave breaking criterion $|q'_y|/\bar{q}_y \geq 2$ (outlined hatched regions), overlaid on the zonal mean zonal winds, for the 10-mb and 1-mb levels.

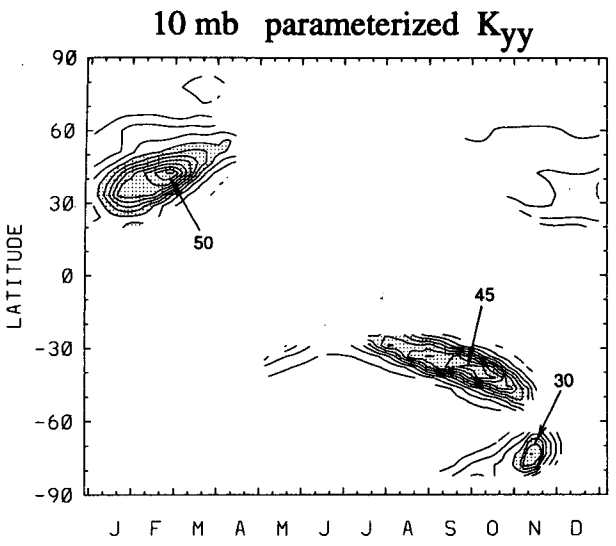

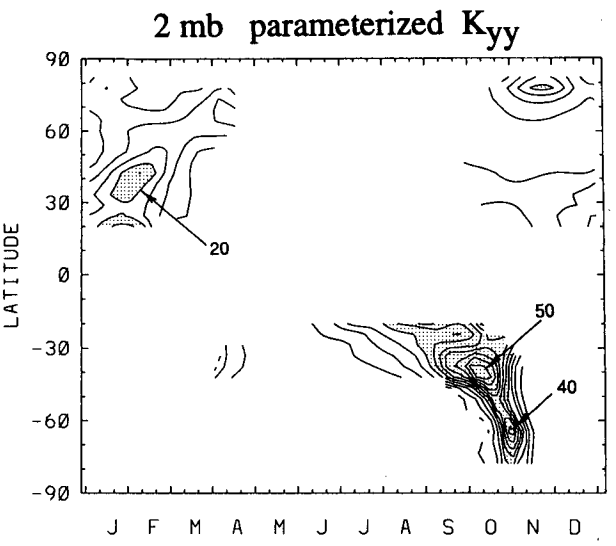

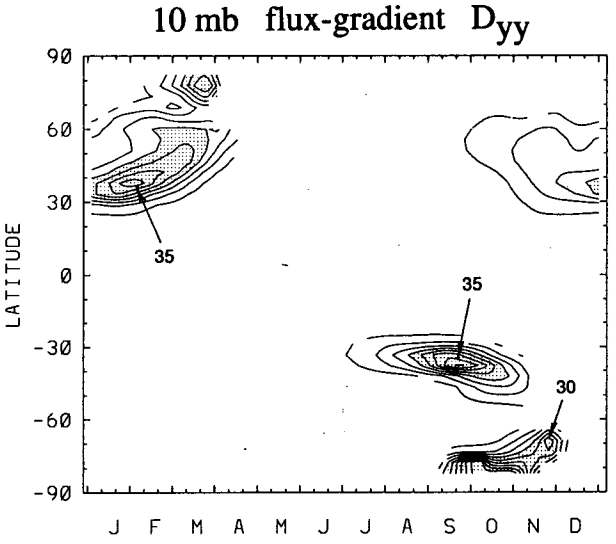

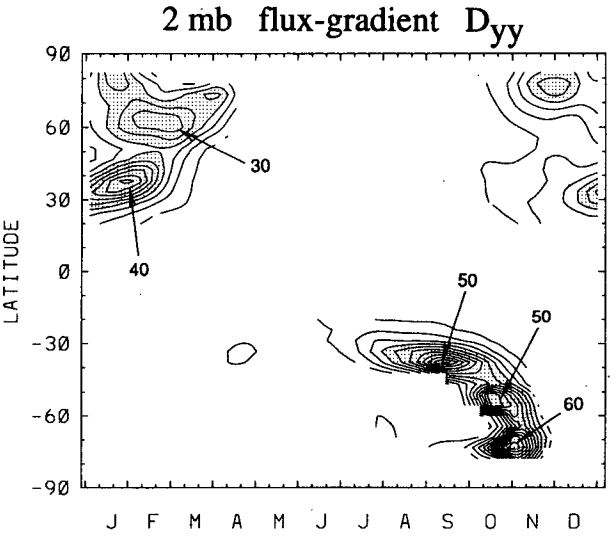

FIG. 12. Climatological latitude–time sections of parameterized, K_{yy}, and flux gradient, D_{yy}, estimates of the diffusion coefficient at 10 mb. Contours are 5×10^5 m^2 s^{-1}, with values above 20 shaded. Values are contoured only over regions where the calculated DF ≤ -0.5 m s^{-1}/day.

FIG. 13. As in Fig. 12 but for the 2-mb level.

determine whether results consistent with the idealized model are obtained. Three central quantities were derived from the data: the wave breaking criterion (19), wave damping rate (10), and parameterized diffusion coefficient (12). Calculations of the wave breaking criterion from observed data clearly identify the subtropical flank of the polar night jet as the primary region of planetary wave breaking. The data suggest that a $|q_y'|/\bar{q}_y$ ratio of 2 be used to quantify such regions. Our results are in good agreement with the calculations of Baldwin and Holton (1988), based on a slightly different wave breaking criterion. The movement of the wave breaking region to higher latitudes during the winter to spring transition documented in this study was also found by Baldwin and Holton for the Northern Hemisphere; here we have shown that similar behavior is found in the Southern Hemisphere. The structure and seasonal evolution of the surf zone observed in these data are in good agreement with the model calculations of G91, which suggests that the observational results may be interpreted in terms of the barotropic instability criterion and the rate of convergence of wave activity into breaking regions.

The damping rates derived here also point to the subtropics as the primary location of the "stratospheric surf zone" during much of the winter season. Maximum damping time scales are found to be 3–4 days,

in good agreement with the damping times derived by G91. Note that nearly identical subtropical wave dissipation rates were derived from the NMC data by Randel (1990) from analysis of *daily* wave activity tendency and EP flux divergence correlations. These similar results validate the use of time-averaged fields in the parameterization scheme. The similarity in the results from the numerical model and from different datasets also supports the idea that group velocity, rather than amplitude, is the fundamental parameter determining the dissipation rate of breaking waves.

The diffusion coefficients, K_{yy}, derived from the parameterization scheme (12) are in reasonable agreement with prior published values, with subtropical maxima in winter of order 30×10^5 m^2 s^{-1}. That the strongest derived mixing occurs in the subtropics, clearly outside the vortex, is consistent with recent analyses of chemical constituent data (Schoeberl et al. 1992). The K_{yy} values calculated here are in good agreement with the estimates, D_{yy}, obtained directly from the flux gradient relationship (14) in the middle stratosphere, but in the upper stratosphere the parameterized K_{yy} values are somewhat smaller. Because a portion of the observed planetary wave EP flux divergence is a result of thermal dissipation rather than wave breaking, Eq. (10) may overestimate significantly the dissipation rate due to breaking in the upper stratosphere, where thermal relaxation is fast. An overestimate of the damping rate due to breaking would then lead to smaller values for the parameterized diffusion coefficient, K_{yy}, compared to the values, D_{yy}, calculated from the flux gradient relationship.

We have shown that when the parameterization of G91 is applied to observational data, estimates of the wave breaking criterion, damping rate, and diffusion coefficient are realistic and are similar to the values calculated with Garcia's model. It might appear at first glance that these similarities are due simply to the fact that the zonal mean state and planetary wave structures calculated with the model compare favorably with stratospheric climatology. However, in G91 the convergence of wave activity, $\nabla \cdot (\mathbf{C}_g A)$, is calculated using the WKB approximation to obtain expressions for $\mathbf{C}_g$ and A, whereas in this study we have used the fact that, for quasigeostrophic waves, $\nabla \cdot (\mathbf{C}_g A)$ is proportional to the EP flux divergence, yet the results for the dissipation rate are essentially the same. Furthermore, the realistic structure and seasonal evolution of the wave and mean fields obtained in G91 are in no small measure a result of the planetary wave breaking parameterization. If the latter is not included in the calculations, the correspondence between model results and observations is much less satisfactory. Thus, the consistency between the results presented here and those of G91 may be taken as support for the ideas that the wave group velocity controls the dissipation rate, δ, and that the latter can be estimated by the WKB method. Finally, insofar as the spatial distribution and magnitude of the parameterized and flux gradient estimates for the diffusion coefficient are similar, our results also validate the use of linear theory to derive the parameterized expression for K_{yy} and provide a theoretical interpretation for the flux gradient relationship (14), which is otherwise an empirical approach to estimating diffusion coefficients from observed data.

Acknowledgments. The authors thank Anne Smith, Joseph Tribbia, and three anonymous referees for their careful and constructive reviews. The manuscript was prepared with the help of Marilena Stone. This work was supported in part under NASA Grants W-16215 and W-15954.

REFERENCES

Andrews, D. G., J. R. Holton, and C. B. Leovy, 1987: *Middle Atmosphere Dynamics.* Academic Press, 489 pp.

Baldwin, M. P., and J. R. Holton, 1988: Climatology of the stratospheric polar vortex and planetary wave breaking. *J. Atmos. Sci.,* **45,** 1123–1142.

Charney, J. G., and M. E. Stern, 1962: On the stability of internal baroclinic jets in a rotating atmosphere. *J. Atmos. Sci.,* **19,** 159–172.

Clough, S. A., N. S. Grahame, and A. O'Neill, 1985: Potential vorticity in the stratosphere derived using data from satellites. *Quart. J. Roy. Meteor. Soc.,* **111,** 335–358.

Dickinson, R. E., 1968: On the exact and approximate theory of vertically propagating planetary Rossby waves forced at a spherical lower boundary. *Mon. Wea. Rev.,* **96,** 405–415.

Garcia, R. R., 1991: Parameterization of planetary wave breaking in the middle atmosphere. *J. Atmos. Sci.,* **48,** 1405–1419.

Haynes, P. H., 1989: The effect of barotropic instability on the nonlinear evolution of a Rossby wave critical layer. *J. Fluid Mech.,* **207,** 231–266.

Juckes, M. N., 1989: A shallow water model of the winter stratosphere. *J. Atmos. Sci.,* **46,** 2934–2955.

Lyjak, L. V., 1987: Diffusion coefficients calculated from satellite data. *Transport Processes in the Middle Atmosphere,* G. Visconti and R. R. Garcia, Eds., D. Reidel, 343–352.

McIntyre, M. E., and T. N. Palmer, 1983: Breaking planetary waves in the stratosphere. *Nature,* **305,** 593–600.

——, and ——, 1984: The 'surf-zone' in the stratosphere. *J. Atmos. Terr. Phys.,* **46,** 825–849.

Newman, P. A., M. R. Schoeberl, R. A. Plumb, and J. E. Rosenfield, 1988: Mixing rates calculated from potential vorticity. *J. Geophys. Res.,* **93,** 5221–5240.

Palmer, T. N., 1982: Properties of the Eliassen–Palm flux for planetary scale motions. *J. Atmos. Sci.,* **39,** 992–997.

Plumb, R. A., and J. D. Mahlman, 1987: The zonally averaged transport characteristics of the GFDL general circulation/transport model. *J. Atmos. Sci.,* **44,** 298–327.

Randel, W. J., 1990: A comparison of the dynamic life cycles of tropospheric medium-scale waves and stratospheric planetary waves. *Dynamics, Transport and Photochemistry in the Middle Atmosphere of the Southern Hemisphere,* A. O'Neill, Ed., Kluwer Academic, 91–110.

——, 1992: Global atmospheric circulation statistics, 1000–1 mb. NCAR Tech. Note, TN-366+STR, 256 pp.

——, and I. M. Held, 1991: Phase speed spectra of transient eddy fluxes and critical layer absorption. *J. Atmos. Sci.,* **48,** 688–697.

Robinson, W. A., 1988: Irreversible wave–mean flow interactions in a mechanistic model of the stratosphere. *J. Atmos. Sci.,* **45,** 3413–3430.

Salby, M. L., R. R. Garcia, D. O'Sullivan, and P. Callaghan, 1990: The interaction of horizontal eddy transport and

thermal drive in the stratosphere. *J. Atmos. Sci.*, **47**, 1647–1665.

Sassi, F., G. Visconti, and J. C. Gille, 1990: Validation of a parameterization scheme for eddy diffusion from satellite data. *J. Atmos. Sci.*, **47**, 2505–2515.

Schoeberl, M. R., L. R. Lait, P. A. Newman, and J. E. Rosenfield, 1992: The structure of the polar vortex. *J. Geophys. Res.*, **97**, 7859–7882.

Smith, A. K., J. C. Gille, and L. V. Lyjak, 1984: Wave–wave interactions in the stratosphere: Observations during quiet and active wintertime periods. *J. Atmos. Sci.*, **41**, 363–373.

Stanford, J. L., J. R. Ziemke, and S. Y. Gao, 1993: Stratospheric circulation features deduced from SAMS constituent data. *J. Atmos. Sci.*, **50**, 226–246.

Yang, H., K.-K. Tung, and E. Olaguer, 1990: Nongeostrophic theory of zonally averaged circulation. Part II: Eliassen–Palm flux divergence and isentropic mixing coefficient. *J. Atmos. Sci.*, **47**, 215–241.